







Open Archive Toulouse Archive Ouverte

OATAO is an open access repository that collects the work of Toulouse researchers and makes it freely available over the web where possible

This is an author's version published in: <http://oatao.univ-toulouse.fr/28127>

Official URL : <https://doi.org/10.1016/j.powtec.2020.10.014>

To cite this version:

Audard, François  and Fede, Pascal  and Belut, Emmanuel and Fontaine, Jean-Raymond and Neau, Hervé  and Simonin, Olivier  *Eulerian modelling of the powder discharge of a silo: Attempting to shed some light on the origin of jet expansion.* (2020) Powder Technology, 379. 49-57. ISSN 0032-5910

Any correspondence concerning this service should be sent to the repository administrator: tech-oatao@listes-diff.inp-toulouse.fr

Eulerian modelling of the powder discharge of a silo: Attempting to shed some light on the origin of jet expansion

François Audard^a, Pascal Fede^{a,*}, Emmanuel Belut^b, Jean-Raymond Fontaine^b, Hervé Neau^a, Olivier Simonin^a

^a Institut de Mécanique des Fluides de Toulouse (IMFT), Université de Toulouse, CNRS, INPT, UPS, FR-31400 Toulouse, France

^b INRS - Laboratoire d'Ingénierie Aérodynamique, FR-54500 Vandoeuvre, France

ARTICLE INFO

Article history:

Received 12 June 2020

Received in revised form 18 September 2020

Accepted 5 October 2020

Available online 09 October 2020

Keywords:

Dust emission

Granular instability

Granular flow

Powder discharge

Frictional viscosity

ABSTRACT

Powder discharging from a silo provokes an emission of dust. To understand and prevent this source of danger, 3D simulations of a silo discharge were performed using an Euler-Euler approach. The impact of the coupling between the flow inside the silo and the granular jet in free-fall is analyzed. Results show that the solid mass flow rate is correctly predicted and that gas back-flowing at the hopper exhaust appears responsible for the formation of a fluctuating and radially expanding jet. However, the radial expansion of the free-falling jet is underestimated. Stochastic fluctuations of the particles velocity at the hopper exhaust are introduced to evaluate their effect on the downstream development of the free-falling jet. These fluctuations are found capable of generating a development of the jet similar to that observed experimentally. This suggests that the granular flow conditions at the hopper exhaust are responsible for the further dispersion of powder.

1. Introduction

When materials in powder form are handled or packaged, it is inevitable that some of them will be dispersed into the surrounding atmosphere. This dispersion can lead to risks of human exposure to dust of hazardous products, to fire and explosion hazards, and to the deposition on surfaces. In turn, this deposition may constitute a secondary cause of risk due to surface contamination and to possible resuspension. Of the phases of powdery materials handling, emptying or filling silos and hoppers are among those that generate the most dust: in that context, computer modelling may be of great help for two stages of the prevention strategy. First, to shed some light on the physical mechanisms at the origin of dust dispersion, which may help finding ways of reducing the risk at its source, and second to design protective means correctly dimensioned to cope with the amount of dispersed dust, which needs to be predicted.

As explained by Cooper and Arnold [1] and Wypych et al. [2], during the discharge of a silo the dust emission may come either from the impact of the granular jet on a stockpile, releasing the entrained air carrying fugitive particles, or from the spreading of the jet during its fall. This study focuses on the second mechanism.

In the literature, many experimental studies on the discharge of a silo were conducted. Some of these were dedicated to the characterization of the granular flow inside the silo [3–5] and others on the

quantification and understanding of the mechanisms responsible of the granular jet spreading [6–11]. These studies showed that the flow rate of induced air into the stream is one of the key to the granular jet expansion. A higher induced flow rate means a higher jet expansion, the air entrained into the core increasing the voidage and reducing the particle fall velocity of the granular jet. Additionally, it has been observed that the incoming air into the free-falling granular jet may lead to a lateral instability [12]. Such a lateral instability can be either attributed to gas-particle or particle-particle interactions. Indeed, Möbius [13]; Royer et al. [14]; Prado et al. [15] found an instability like the Rayleigh-Plateau instability observed in the fluid jet. This instability appears even without air and could be provoked by a cohesion effect linked to the humidity and particle charge. The authors proposed the introduction of an effective granular surface tension to describe such an instability [14,16,17]. However, the instability could also find its origin at the granular flow transition at the opened bottom of the silo, or in the granular flow inside the silo (non-sphericity of particles, wall roughness, particle-wall interactions or arches formation).

In this study, we performed numerical simulations of the discharge of powder from a silo as an attempt to clarify the mechanisms at the origin of powder jet expansion, with a focus on the coupling between the flow inside the silo and in the free-fall zone. The numerical simulation of particle-laden flows can be performed by several approaches. First, the Euler-Lagrange approach where the fluid flow is represented by the Direct Numerical Simulation (DNS), or Large Eddy Simulation (LES), of the Navier-Stokes equations. Another way for representing the fluid is to solve the Reynolds Average Navier-Stokes (RANS) where a closure

* Corresponding author.

E-mail address: pascal.fede@imft.fr (P. Fede).

law is needed for the turbulent dispersion. The particles are tracked individually in a Lagrangian framework and the inter-particle collisions are taken into account by a Discrete Element Method (DEM). The second approach to numerically simulate a particle-laden flow is the Euler-Euler approach, also called Two-Fluid Method (TFM), where both phases are treated as continuous phase. In the literature the Euler-Lagrange approach has been extensively used for the numerical simulations of the silo discharge but only for investigating the flow inside the silo [18,19]. Concerning the TFM approach, the numerical simulation of the granular flow inside the silo is challenging because it requires additional closure to take into account the frictional effect. Vidyapati and Subramaniam [20] made a quantitative comparison of DEM and different constitutive models in TFM. Zhou et al. [21] also did such a comparison but with also some experimental data and with another rheology for the frictional stress. For the spreading of the free-falling granular jet, only a few studies can be found. Uchiyama [22] performed 2D Euler-Lagrange numerical simulation of the experiment conducted by Ogata et al. [9]. More recently, Chu et al. [23] reported 3D Euler-Lagrange simulations of the case described by Liu et al. [8].

In all these studies, the coupling between the granular flow inside the silo and its consequences on the spreading of the free-falling jet was not investigated. To analyze this coupling, 3D Euler-Euler numerical simulations with and without a silo were performed. The configuration is the well-documented silo discharge experiment made by Ansart et al. [6]. The details of the geometry and numerical approach are given in Section 2. The analysis of the coupling between the granular jet spreading and the granular flow inside the silo is analyzed in Section 3. Finally, in Section 4 a stochastic model is proposed for representing the perturbations of the granular flow at the nozzle. Conclusions are drawn in the last section.

2. Numerical simulation overview

We consider the setup studied experimentally by Ansart et al. [6], which is composed of a silo and a dispersion chamber.

The silo consists of an upper cylindrical part (height 600 mm, diameter 200 mm) which ends at its bottom with a hopper. This hopper consists of a downward narrowing conical section (height 190 mm, half-angle 30, adjustable exhaust diameter). The nozzle penetrates inside the dispersion chamber by 34.64 mm and the thickness of the nozzle is 10 mm (see Fig. 3). The dispersion chamber is made of two parts, the upper part consists of a cylinder (radius 250 mm, height of 500 mm), and the lower part of a parallelepiped volume (section $600 \times 600 \text{ mm}^2$, height 814 mm). A plate (thickness 10 mm), pierced with a circular hole (diameter 240 mm), is placed 200 mm above the bottom of the parallelepiped part of the chamber. The region of interest of the powder discharge is situated above that plate, which prevents particles reaching the bottom of the chamber from going backward above the plate. As shown by Fig. 1, the setup presents six air inlets: two at the top of the silo, two at the middle of the chamber and two at the bottom of the chamber. At the top of the parallelepiped part, the area of the two air inlets is 520.51 mm^2 . (See Fig. 2.)

To investigate the dense to dispersed solid-gas flow in the experimental setup of Ansart et al. [6], 3D transient numerical simulations of the experiment were conducted by means of an Eulerian multi-fluid modelling approach for gas and solid interaction developed and implemented by IMFT (Institut de Mécanique des Fluides de Toulouse) in the NEPTUNE_CFD software, based on the open-source software Code_Saturne. This software is a multiphase flow solver developed in the framework of the NEPTUNE project, financially supported by CEA, EDF, IRSN and Framatome. The numerical solver has been developed for High Performance Computing [24–26]. The transport equations are derived by phase ensemble averaging for the continuous phase and in the framework of the kinetic theory of granular flows [27] for the dispersed phase but extended in order to take into account the interstitial fluid effects and particles-turbulence interactions [28,29]. The

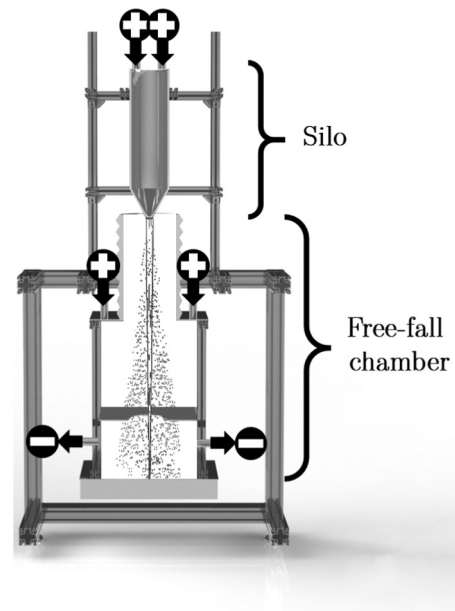


Fig. 1. Experimental setup of Ansart et al. [6]. The sign “+” means that the surrounding air enters inside the domain and “-” means that the flow is going outside the domain.

fluid-particle momentum transfers are taken into account by the model proposed by Gobin et al. [30]. The turbulence of the gas phase is computed using the $k - \varepsilon$ model and extended for gas-particle flow by taking into account the reverse coupling terms between phases [31]. Particle kinetic agitation is treated by the model $q_p^2 - q_{fp}$ which solved a transport equation for the particle agitation $q_p^2 = 1/2 \langle u_{p,i} u_{p,i} \rangle$ and for the fluid-particle covariance $q_{fp} = \langle u_{p,i} u_{f,i} \rangle$ (the prime denote the fluctuating velocities). The model takes into account the agitation transfer from the gas turbulence to the particulate phase and the inter-particle collisions). The full description of the mathematical model can be found in Boëlle et al. [32]; Simonin [29]; Fede et al. [33]. As explained in the introduction, the particulate flow regime

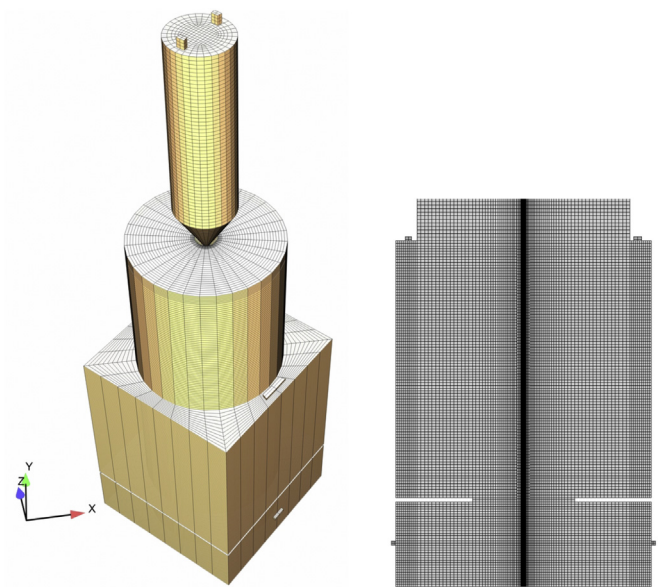


Fig. 2. Three dimensional (left) and slice view (right) of the mesh (z-axis is along the central axis of the silo). The mesh contains 414,000 hexahedra cells for the chamber and 17,000 cells for the silo.

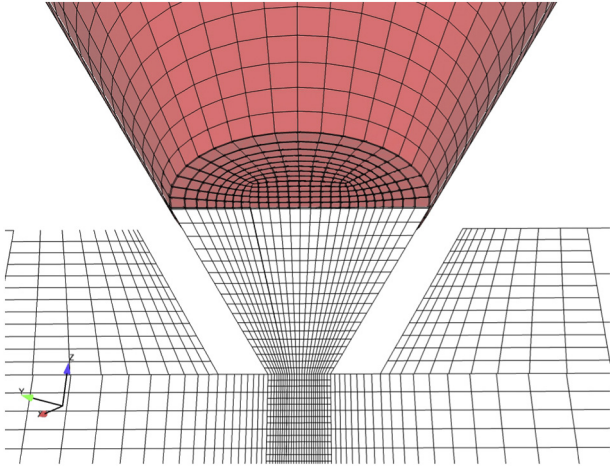


Fig. 3. Mesh of the nozzle.

passes from quasi-static to dilute flows. Then the frictional effects have to be taken into account in the modelling approach especially in regions where the solid phase is dense as in the silo. In the present study, a frictional contribution has been added to the particle kinetic stress tensor in momentum equation. The model for frictional effects has been proposed by Johnson et al. [34] for the pressure and Srivastava and Sundaresan [35] for the viscosity details can be found in Bennani et al. [36]. Basically the frictional pressure is given by

$$p^{fr} = \begin{cases} F \frac{(\alpha_p - \alpha_{p, min})^r}{(\alpha_{p, max} - \alpha_p)^s} & \text{if } \alpha_p > \alpha_{p, min} \\ 0 & \text{if } \alpha_p \leq \alpha_{p, min} \end{cases}$$

where $F = 0.05 \text{ Pa}$, $r = 2$, $s = 5$, $\alpha_{p, min} = 0.5$ and $\alpha_{p, max} = 0.64$. The frictional stress tensor is obtained by

$$\Sigma_{ij}^{fr} = p^{fr} \delta_{ij} - \sqrt{2} \sin(\phi) p^{fr} \frac{S_{ij}}{\sqrt{\underline{S} : \underline{S} + \frac{8}{3} d_p^2}}$$

with d_p the particle diameter, q_p^2 the particle agitation that is computed by the resolution of a transport equation (see for example Fede et al. [33]) and $\phi = 28.5^\circ$ the internal friction angle. The strain rate of deformation is defined as $S_{ij} = \frac{\partial U_{p,i}}{\partial x_j} + \frac{\partial U_{p,j}}{\partial x_i} - \frac{2}{3} \frac{\partial U_{p,k}}{\partial x_k} \delta_{ij}$ with $U_{p,i}$ is the mean particle velocity. We emphasize that more sophisticated models exist for the frictional stress tensor as Benyahia [37]; Schneiderbauer et al. [38]; Chialvo et al. [39]. However, as shown in the next section, such a simple model leads to good predictions of the solid mass flow rate at the nozzle.

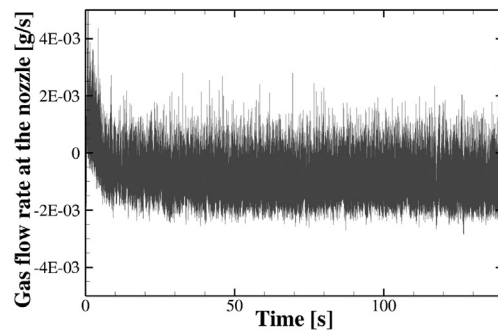
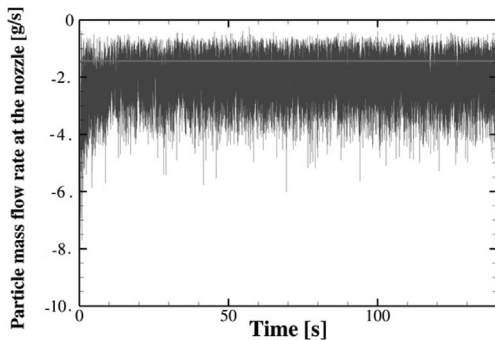


Fig. 4. Flow rate time series for particles (left) and gas (right) at the hopper exhaust obtained for simulations with silo. The green horizontal solid line corresponds to the time-averaged value of the experimental solid mass flow rate. Flow rates are negative when directed outside the silo.

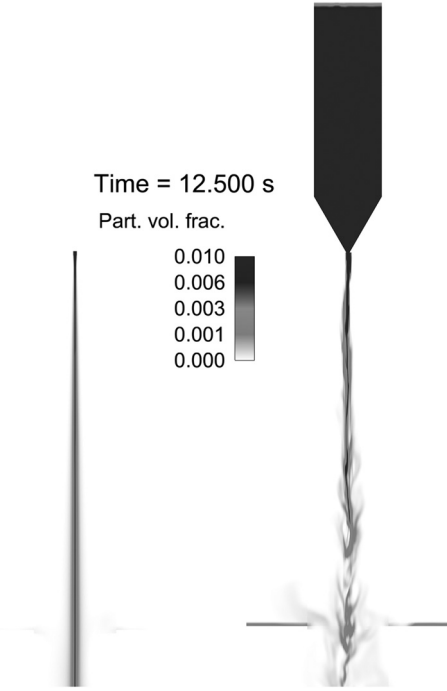


Fig. 5. Instantaneous fields of particles volume fraction, for simulations without the silo (left) and with the silo (right). Slice cut of a 3D view.

The computational grid used in this study is shown by 2 & 3 where the silo, the chamber, the plate and the air inlets are represented. The domain was discretized with 414,000 hexahedral cells for the chamber and 17,000 cells for the silo. The mesh is locally refined close to the vertical central axis. A mesh-sensitivity analysis has been conducted in order to have a mesh-independent results.

Numerical simulations were carried out either with or without the silo. In the first case, the silo is initially filled with a particle volume fraction of 60% and the particle and air mass flow entering the dispersion chamber is computed by the simulation. In the second case (i.e. without silo), the particle mass flow rate entering the chamber was set to $1.44 \text{ g} \cdot \text{s}^{-1}$, according to measurements, and the gas mass flow rate to $1.44 \times 10^{-3} \text{ g} \cdot \text{s}^{-1}$ assuming a particle volume fraction of 0.56 at inlet. The main numerical parameters are gathered in Table 1. An adaptive time-step has been used based on a maximum value of Fourier number of 10 and a maximum value of the Courant number of 1. It leads to an averaged time-step about $5 \times 10^{-4} \text{ s}$.

Air inlets were numerically described as free inlets, meaning zero normal derivative for the velocities and Dirichlet conditions for the

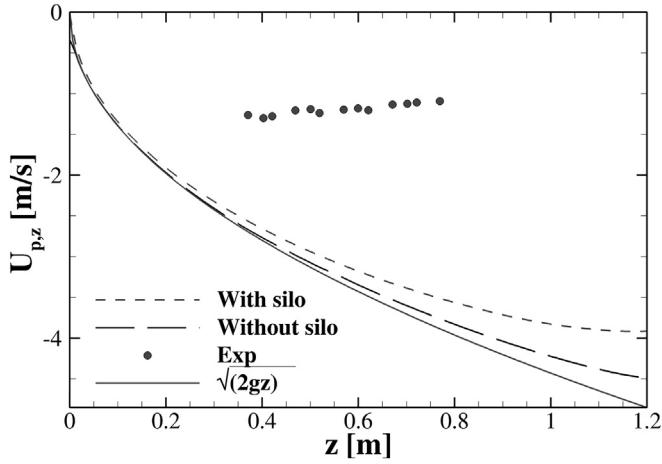


Fig. 6. Mean axial particle velocity along the central z axis in the chamber. Dashed lines represent simulation results, the solid line represents the free-fall settling velocity ($\sqrt{2gz}$) and symbols correspond to experimental data from Ansart et al. [6].

pressure and solid volume fraction. The stop pressure P_{ref} is imposed according to $P_{in} = P_{ref} - 1/2\rho_f U_{in}^2$ where U_{in} is the gas velocity at the inlet, and ρ_f the fluid density. The bottom surface of the domain corresponds to a free outlet boundary condition for the particulate phase (to avoid particle accumulation) and is a wall for the gas phase. The gas can flow out of the domain by the two gas outlets located at the bottom of the domain for those free outlet boundary conditions are imposed meaning that zero flux is imposed on all computed variables except for the pressure that is imposed. As shown by Audard et al. [40], the wall boundary conditions used in the silo are particularly important for the correct prediction of the particle mass flow rate at the hopper exhaust. On the contrary, wall boundary condition type (slip, friction or no-slip) used in the chamber does not affect the gas-solid flow in the domain. Consequently, the wall boundary condition in the domain is respectively no-slip for the particulate phase and friction for the gas [33].

Each numerical simulation corresponds to 130 s of physical time. During the first 50 s, the flow develops in the dispersion chamber before reaching a statistically steady state. Time-averaged statistics are then computed during the following 80 s of physical time.

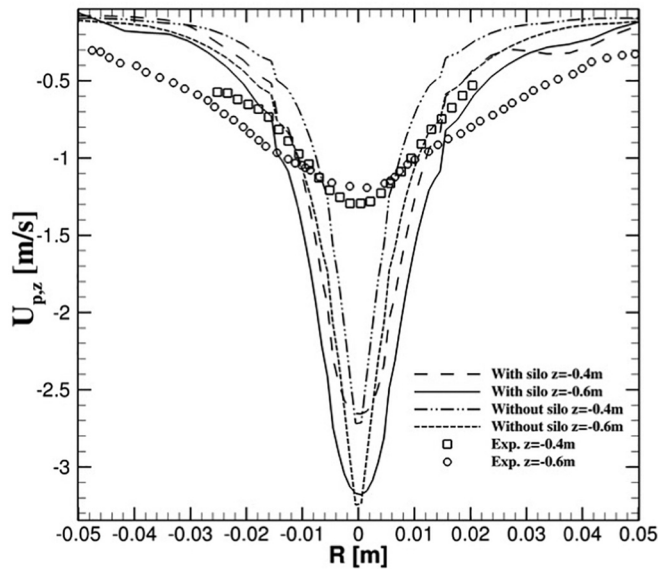


Fig. 7. Radial profile of the mean axial particle velocity measured at several distances from the nozzle. The symbols are the cases without the silo and the lines with the silo.

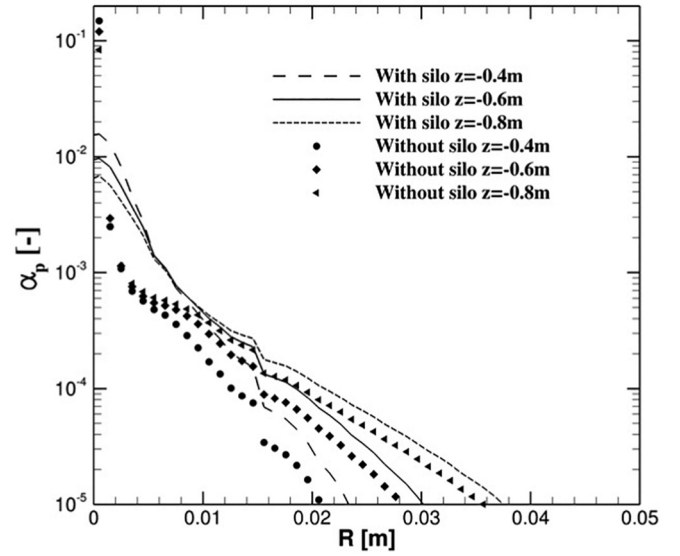


Fig. 8. Radial profile of the mean particle volume fraction measured at several distances from the nozzle. The symbols are the cases without the silo and the lines with the silo.

3. Effect of flow coupling between the silo and chamber

In this section, simulation results regarding the coupling between the flow in the silo and in the dispersion chamber are examined. Before to enter in details of the analysis, it must be emphasized that the granular flow is critical according to the definition given by Gidaspow [41]. Indeed, we did not observe any effect of the downstream conditions on the granular flow inside the silo. In fact, the gas solid volume fraction waves created in the dispersion chamber do not propagate upstream back inside the silo.

Fig. 4 shows the solid and gas mass flow rates predicted at the hopper exhaust. Time-averaged values are reported in Table 2. The particle mass flow rate is correctly predicted by the model when the silo is taken into account (3% variation with respect to the reported experimental value). As shown by Fig. 4, large fluctuations of solid mass flow rate reaching circa 30% of mean are predicted by simulations. These

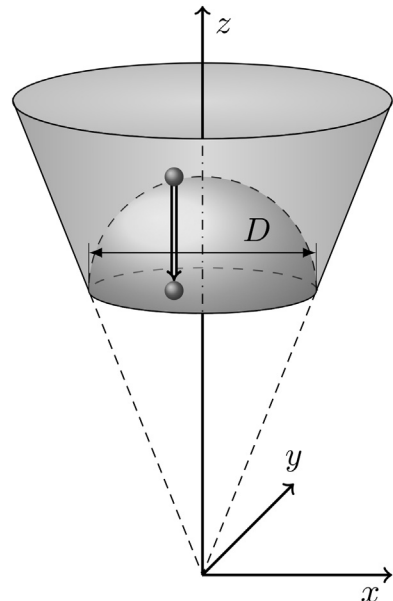


Fig. 9. Representation of the free-fall zone by an hemispherical shape.

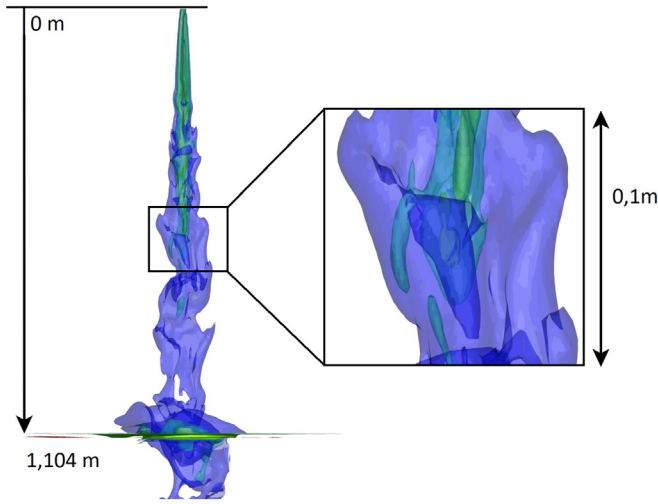


Fig. 10. Instantaneous particle volume fraction obtained with a perturbation at the hopper exhaust, for a simulation without upstream silo (forcing variance $\langle u'^2 \rangle = 0.004 \text{ m}^2 \cdot \text{s}^{-2}$ and timescale $\tau = 4\tau_p$). Right view focuses on the region situated at a distance of 0.5 m with respect to the hopper.

fluctuations correspond to the perturbations of the granular jet and to the formation of clusters illustrated by Fig. 5. Whereas the solid mass flow rate exhibits only negative - however fluctuating - values, the gas mass flow rate presents both negative and positive values, meaning that gas sometimes back-flows at the hopper exhaust.

The air mass flow rate Q_g^{Top} entering through the upper inlets of the silo balances the volumetric losses in the silo due to air and particles

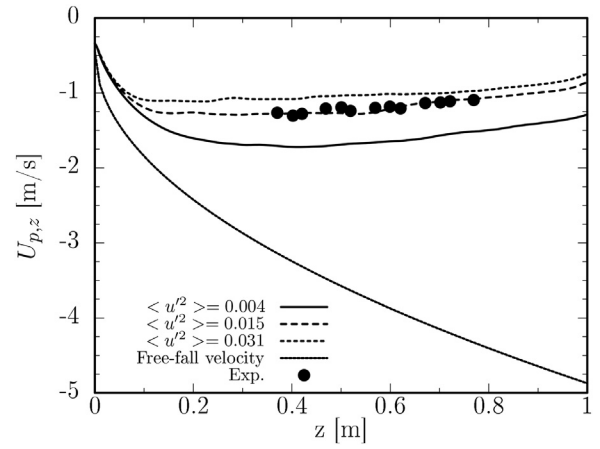


Fig. 13. Axial mean velocity of particle profiles obtained for different forcing variances $\langle u'^2 \rangle$. Particles free fall velocity in vacuum is also represented as a reference.

leaving the silo by the hopper exhaust hence $Q_g^{Top} = Q_g^{Nozzle} + Q_p^{Nozzle} \rho_g / \rho_p$. The gas that backflows at the hopper exhaust disturbs the flow of particles leaving the silo and probably provokes the solid mass flow rate fluctuations (similarly to an emptying bottom-up bottle of liquid). Without the silo, the velocity and volume fraction of air and particles leaving the hopper exhaust are prescribed and constant, no backflow consequently occurs. In this case, the granular jet in the dispersion chamber does not exhibit any perturbation, as shown by Fig. 5. Fig. 6 shows the mean particle vertical velocity predicted along the central vertical axis. When the silo is not taken into account in the modelling, the particle velocity is almost equal to the free-fall velocity

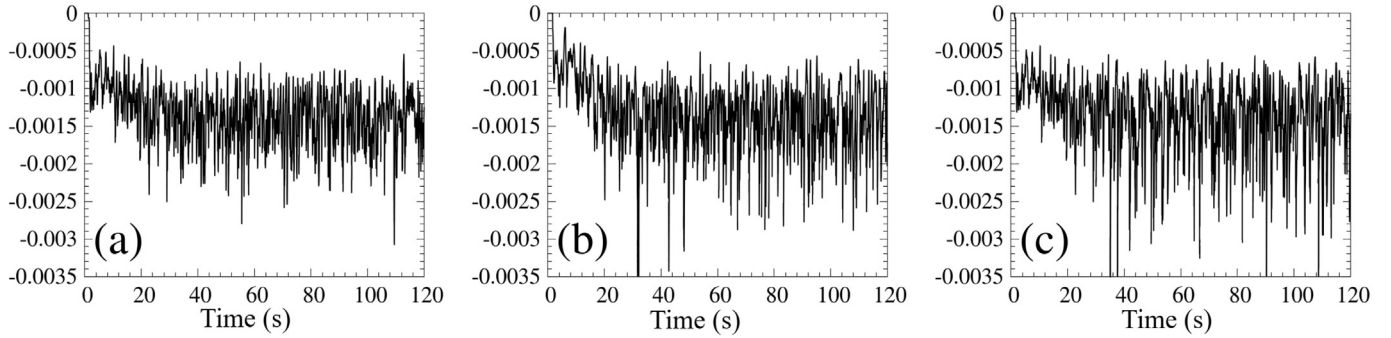


Fig. 11. Mass flow rate of particles leaving the simulated domain by its bottom end, Q_{out} in $\text{kg} \cdot \text{s}^{-1}$. From left to right $\langle u'^2 \rangle = 0.004 \text{ m}^2 \cdot \text{s}^{-2}$ (a); $\langle u'^2 \rangle = 0.015 \text{ m}^2 \cdot \text{s}^{-2}$ (b); $\langle u'^2 \rangle = 0.031 \text{ m}^2 \cdot \text{s}^{-2}$ (c).

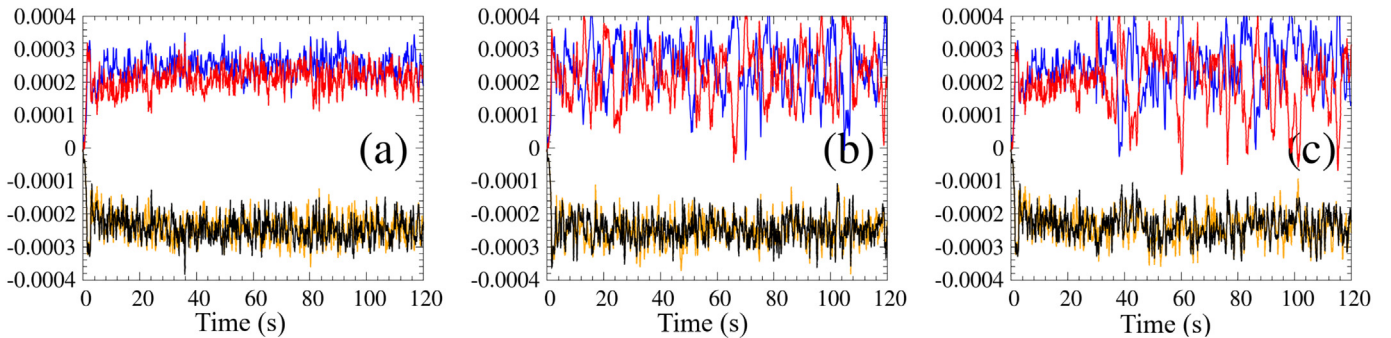


Fig. 12. Time series of the gas mass flow rate at the vents, for $\langle u'^2 \rangle = 0.004 \text{ m}^2 \cdot \text{s}^{-2}$ (a); $\langle u'^2 \rangle = 0.015 \text{ m}^2 \cdot \text{s}^{-2}$ (b); $\langle u'^2 \rangle = 0.031 \text{ m}^2 \cdot \text{s}^{-2}$ (c). Lines — — correspond to the middle vents of the chamber and lines — — correspond to the lower vents.

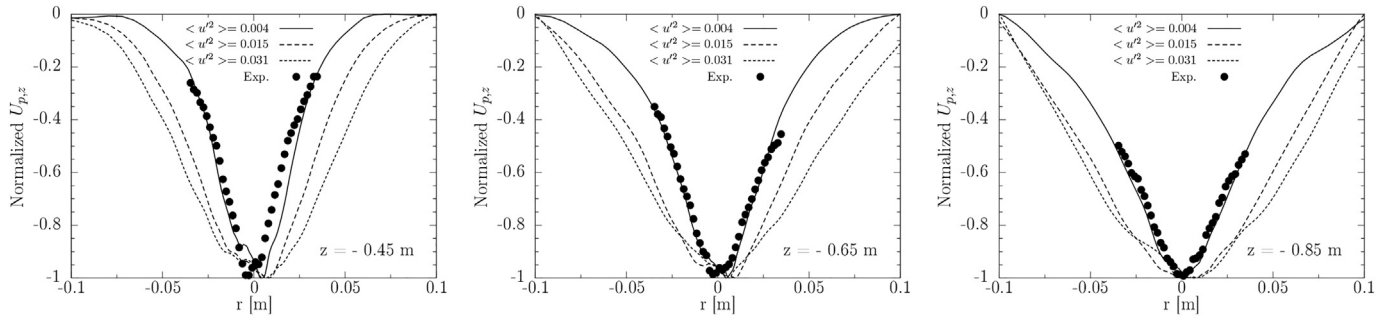


Fig. 14. Radial profiles of particles vertical velocity, normalized by its value along the central z -axis, for different values of the forcing variance $\langle u'^2 \rangle$. Each sub-figure correspond to a different z distance to the hopper exit.

of particles in vacuum. When the silo is taken into account, the magnitude of the particle velocity is slightly decreased but remains larger than the one measured experimentally.

Radial profiles of mean vertical particle velocity and solid volume fraction are shown by Figs. 7 & 8. Compared to experiments, the granular jet is narrower in simulations and its span is much smaller. Hence, even if the jet exhibits solid volume fraction fluctuations at the hopper exhaust when the silo is simulated, these fluctuations are apparently not sufficient to produce the downstream widening of the air and particle jet in the dispersion chamber.

In this section, we showed that the air and particle flows inside the dispersion chamber are both conditioned by the upstream flow inside the silo. The gas back-flowing at the hopper exhaust indeed produces temporal fluctuations of the particulate mass flow rate leaving the silo. These fluctuations appear responsible for the lateral spreading of the particles downstream. These results are in accordance with the phenomenological description of falling powder jets made by Cooper and Arnold [1] and later by or Liu et al. [8].

However, even if considering the gas and particle flow in the upstream silo in our simulations allows reproducing the experimental particle mass flow rate at the hopper exhaust and a convincing particle jet destabilization, the numerical simulations with silo still exhibit too large particle vertical velocity and too small radial expansion of the granular jet compared to experiments. The expansion of the granular jet is indeed only slightly enhanced when the silo is taken into account. The perturbations induced by the gas back-flow do not seem sufficient to disperse significantly the jet and thus decrease the particles fall velocity.

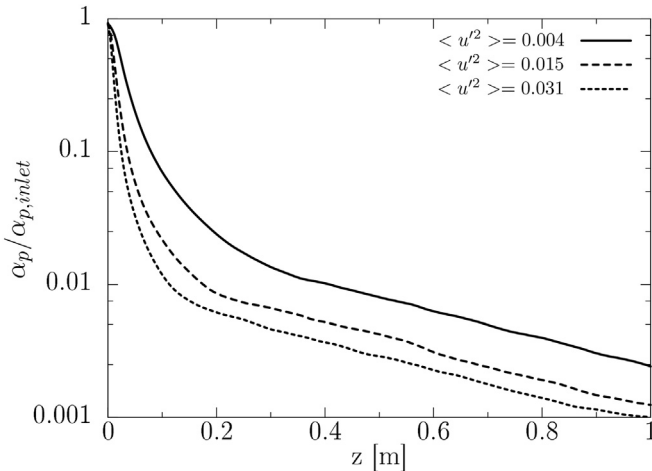


Fig. 15. Particle volume fraction normalized by the volume fraction at the inlet for different forcing variances.

Another possible origin of large destabilization of the gas and particles velocities and volume fractions at the hopper exhaust could be a hysteresis phenomenon such as intermittent particles arches and avalanches in the silo. This phenomenon is not taken into account in present Eulerian multi-fluid model. To investigate the effect of such phenomenon, the next section proposes to examine the consequences of adding a synthetic perturbation at the entrance boundary condition for particles in simulations without silo.

4. Effect of a perturbation on the dispersion of the granular jet

To represent the fluctuations induced by arches or avalanches at the exhaust of the hopper, a perturbation is added in the simulation without silo. More precisely the perturbation is added at the inlet boundary condition that is located at the silo nozzle. Basically the perturbation can be applied on the particle velocity or on the solid volume fraction. In the present study the perturbation is imposed on the particle velocity and more precisely it is imposed only on the radial component of the particle velocity at the inlet. Tests have been conducted by adding the perturbation also on the vertical component but without significant effect on the granular jet spreading. The nature of the perturbation is also important and here we have chosen a Langevin scheme because it has a temporal correlation like probably the phenomena that we try to mimic namely arches and avalanches.

Using a first order numerical scheme, the perturbation is then imposed as

$$U_{p,r}^{n+1} = U_{p,r}^n \left(1 - \frac{\Delta t}{\tau} \right) + \hat{\xi} \sqrt{\frac{2\langle u'^2 \rangle}{\tau}} \Delta t \quad (1)$$

where $U_{p,r}$ is the radial component of the particle velocity at the inlet, Δt the simulation time-step, τ the integral time scale of the process, $\langle u'^2 \rangle$ the variance of the process and $\hat{\xi}$ is a random number drawn in a normal distribution. To use Eq. (1) four parameters are needed: an initial vertical particle velocity, an initial solid volume fraction (these two are coupled in order to fit the experimental solid mass flow rate) and two new parameters for the stochastic forcing, namely $\langle u'^2 \rangle$ and τ .

The particle vertical inlet velocity is deduced from the experiment where only the particle mass flow rate leaving the hopper was

Table 1
Parameters of the numerical simulations.

Air	Density, ρ_f	1.2 kg. m ⁻³
	Viscosity, μ_f	1.85 × 10 ⁻⁵ Pa. s
Particles	Density, ρ_p	1000 kg. m ⁻³
	Mean diameter, d_p	60 μm
	Restitution coefficient, e_c	0.9
	Mass flow rate through the nozzle, \dot{m}	1.44 × 10 ⁻³ kg. s ⁻¹
Geometry	Nozzle diameter, D	10 mm

Table 2

Time-averaged mass flow rates (in $\text{g} \cdot \text{s}^{-1}$) obtained in numerical simulations. The negative value means that the gas is flowing out, to the dispersion chamber.

		Experiment	w/o silo	w silo
Nozzle	Part.	1.440	1.440	1.482
	Air Whole	-	1.440×10^{-3}	-1.467×10^{-3}
	Air Upw.	-	-	0.362×10^{-4}
	Air Downw.	-	-	-1.483×10^{-3}
Air inlet	Top	-	-	3.285×10^{-3}
	Mid.	-	70.12×10^{-3}	68.30×10^{-3}
	Bot.	-	-71.55×10^{-3}	-69.71×10^{-3}

measured. Hence the corresponding particle volume fraction and the particle velocity are not separately known. To set the velocity of particles entering in the dispersion chamber, we consider that during emptying, arches and/or avalanches may be present. In that case, the particles velocity at the outlet of the hopper can be reduced with respect to Beverloo et al. [42] predictions by a factor of typically 2 to 10 [43]. In that context, Brown and Richards [44] proposed to describe the flow at the outlet of the hopper by introducing an imaginary *free-fall zone*. This zone presents a hemispherical shape (see Fig. 9) of identical diameter than the hopper outlet. From this representation, the velocity of particles leaving the hopper is determined by assuming that particles fall freely and isolately through this free-fall zone.

Hence the vertical inlet particle velocity reads

$$U_{p,vert} = \sqrt{2gh} \quad (2)$$

with $h = D/2$. In the considered experimental setup, the corresponding particle vertical velocity at the hopper outlet is $U_{p,vert} = 0.313 \text{ m} \cdot \text{s}^{-1}$. The particle volume fraction $\alpha_{p,inlet}$ at the hopper outlet is deduced from the experimental solid mass flow rate, consequently $\alpha_{p,inlet} = 0.0585$.

As regards the time parameters of the perturbation, three variances on transverse velocity were investigated, respectively $\langle u'^2 \rangle = 0.0039, 0.015625$ and $0.03125 \text{ m}^2 \cdot \text{s}^{-2}$. These variances correspond to amplitudes of variation of the particles inlet velocity respectively equal to 0.083, 0.15 and $0.25 \text{ m} \cdot \text{s}^{-1}$. The timescale τ was set to $\tau = 4\tau_p$ where $\tau_p = \rho_p d_p^2 / 18\mu_f$ is the Stoke's particle response time. This value was chosen because it leads to a perturbation frequency of about 25 Hz, which corresponds to that observed experimentally [6].

As first results, Fig. 10 shows the instantaneous solid volume fraction obtained while imposing a stochastic perturbation at the hopper exhaust in simulations without silo. In contrast with a similar case without perturbation (Fig. 5, left), the granular jet is destabilized and the formation of clusters is visible.

4.1. Gas and solid mass flow rate

Fig. 11 shows the time-evolution of the particle mass flow leaving the simulated domain by its lower end, for each considered variance of the Langevin perturbing process $\langle u'^2 \rangle$. The temporal standard deviations of these mass flow rates are compared in Table 3. When $\langle u'^2 \rangle$ decreases, the standard deviation of the mass flow rate of particles exiting the domain decreases. The time evolution of the gas mass flow rates at the vents (Fig. 12) follows a behaviour similar to that of the mass flow rate of exiting particles. For large values of $\langle u'^2 \rangle$, the gas mass flow

Table 3

Standard deviation of the particles mass flow rate at the exit (bottom) of the domain for a random perturbation of particles inlet velocity generated by a Langevin process.

τ [s]	$\langle u'^2 \rangle$ [$\text{m}^2 \cdot \text{s}^{-2}$]	$\sigma_{Q_{out}}$ [$\text{g} \cdot \text{s}^{-1}$]
$4\tau_p$	0.004	0.3465
$4\tau_p$	0.015	0.4226
$4\tau_p$	0.031	0.476

rate at the vents is not always positive, air either entering or leaving the dispersion chamber through the vents. In such situations, the variations of air mass flows at the air inlets are in phase opposition.

4.2. Particle vertical velocity

The mean z-velocity of particles along the central z-axis of the jet of falling particles is shown on Fig. 13. When the variance of the perturbation decreases, the vertical z-velocity of particles increases. Whichever the considered variance, all particles vertical velocity profiles along the central z-axis of the jet are close to the experimental values. In the case of an intermediate variance ($\langle u'^2 \rangle \approx 0.015 \text{ m}^2 \cdot \text{s}^{-2}$) simulated velocities match the measurements.

Radial profiles of particles vertical z-velocity at several z positions are shown on Fig. 14. The best match with experimental measurements is found for $\langle u'^2 \rangle = 0.004 \text{ m}^2 \cdot \text{s}^{-2}$, i.e. for a different value of the parameter $\langle u'^2 \rangle$ that led to a match of simulated and measured values of the central z-velocity. It is apparent however that the destabilization procedure presented in this section makes it possible to reproduce the experimentally observed radial decrease of particles fall velocity, and its dependence with respect to the distance to the hopper exit. Profiles close to that measured experimentally by Ansart et al. [6] are indeed obtained.

4.3. Solid volume fraction

The evolution of the volume fraction normalized by the volume fraction at the hopper exhaust is shown on Fig. 15. The particle volume fraction decreases with the distance to the hopper, a higher variance of the stochastic perturbation process leading to a higher decrease slope of $\alpha_p/\alpha_{p,0}$. This traduces the widening effect of the intensity of the initial perturbation on the development of the particle jet, a higher initial variance leading to a more rapidly diluting jet.

5. Conclusions

The free fall of powder particles discharging from a silo was numerically investigated by means of a two-fluids model. Basing ourselves on the experimental situation reported Ansart et al. [6], we evaluated the effect of various modelling strategies on the reproduction of velocity profiles of falling particles, of the spreading rate of the powder jet and of the induced air flow rate.

When the granular flow in the upstream silo and its coupling with the dispersed flow in the free-fall chamber were considered, using the frictional model proposed by Srivastava and Sundaresan [35]), simulations predicted the correct solid mass flow rate at the hopper exhaust. In that case, we observed that time-varying instabilities of air and particle velocity and volume fraction appear at the exhaust of the hopper. These instabilities are apparently linked with the existence of air intermittently back-flowing from the dispersion chamber into the hopper. As the particulate jet falls in the chamber, these initial instabilities lead to the jet radial dispersion, through the apparition of detached particles clusters: the mean particles jet widens with the fall distance. These observations are in qualitative accordance with the experimental results of Ansart et al. [6], as well as with the phenomenological description of falling powder jets made by Cooper and Arnold [1] or Liu et al. [8]. However, the spread angle of the jet is largely underestimated with respect to measurements.

When the upstream granular flow in the silo is not taken into account in simulations, the most straightforward simulation strategy consists of assuming that the velocities and volume fraction of particles entering the dispersion chamber can be simply deduced from the mass flow rate of discharged particles and from the volume fraction in the silo. In doing so, we observed a minimal widening of the particle jet with no time-varying fluctuations. The vertical velocity of particles along the centerline of the jet is then identical to that of particles falling

freely in vacuum. These results do not correspond to the experimental behaviour.

To shed some more light on the phenomenon that could be at the origin of the particle jet expansion in the chamber, we proposed to add a simple stochastic forcing on the radial velocity of particles entering the dispersion chamber, for simulations without silo. In order to take into account a possible temporal correlation, a Langevin process was considered. The characteristic timescale of the process was chosen from the experimental data and the sensitivity to the forcing variance was investigated. We observed that choosing the proper variance of the perturbing process allowed reproducing the expected behaviour of the particle jet, in terms of spreading angle, fall velocity and flow rate of entrained air. However, all these properties could not be reproduced simultaneously with a single value of the forcing variance. We may extrapolate that some more sophisticated forcing disturbance could lead to the proper development of the air and particle jet.

Generally speaking, these various simulation attempts highlight the key role of the granular flow at the hopper exhaust on the further dispersion of the jet of particles in the free-fall chamber. Thus, a dense and regular flow of particles at the hopper exhaust leads to no dispersion and no air entrainment, while an intermittent and dilute flow leaving the hopper leads to a particulate jet that widens, entraining the surrounding air and dispersing particles.

If the employed frictional model does apparently not reproduce the effective instabilities of the powder flow leaving the hopper, it could be interesting in further work to evaluate more sophisticated models such as those proposed by Jop et al. [45] or Schneiderbauer et al. [38]. However, these models do not include mechanisms like arches formation of avalanches and these phenomena clearly may induce the kind of fluctuations of particles velocity and volume fraction at the hopper exhaust that lead to the dispersion of the particle jet in the chamber.

Declaration of Competing Interest

The authors declare that they have no known competing financial interests or personal relationships that could have appeared to influence the work reported in this paper.

Acknowledgements

This work was granted access to the HPC resources of CALMIP supercomputing center under the allocation 2020-0111. This work was performed using HPC resources from GENCI-CINES (Grant 2015-c20152b6012). Authors thank Dr. Ansart for fruitful discussions.

References

- [1] P. Cooper, P. Arnold, Air entrainment and dust generation from a falling stream of bulk material, *KONA Powder Particle J.* 13 (1995) 125–134, <https://doi.org/10.14356/kona.1995017>.
- [2] P. Wypych, D. Cook, P. Cooper, Controlling dust emissions and explosion hazards in powder handling plants, *Chem. Eng. Process. Process Intensif.* 44 (2005) 323–326, <https://doi.org/10.1016/j.cep.2004.02.026>.
- [3] M. Benyamine, M. Djermane, B. Dalloz-Dubrujeaud, P. Aussillous, Discharge flow of a bidisperse granular media from a silo, *Phys. Rev. E* 90 (2014), 032201, <https://doi.org/10.1103/PhysRevE.90.032201>.
- [4] Y. Zhou, P.Y. Lagrée, S. Popinet, P. Ruyer, P. Aussillous, Gas-assisted discharge flow of granular media from silos, *Phys. Rev. Fluids* 4 (2019) 124305, <https://doi.org/10.1103/physrevfluids.4.124305>.
- [5] Y. Zhou, P. Ruyer, P. Aussillous, Discharge flow of a bidisperse granular media from a silo: discrete particle simulations, *Phys. Rev. E* 92 (2015), 062204, <https://doi.org/10.1103/PhysRevE.92.062204>.
- [6] R. Ansart, A. de Ryck, J.A. Dodds, M. Roudet, D. Fabre, F. Charru, Dust emission by powder handling: comparison between numerical analysis and experimental results, *Powder Technol.* 190 (2009) 274–281, <https://doi.org/10.1016/j.powtec.2008.04.053>.
- [7] W. Cao, H. Liu, W. Li, J. Xu, The characteristics of the near field of the granular jet, *Fuel* 115 (2014) 17–23, <https://doi.org/10.1016/j.fuel.2013.07.010>.
- [8] Z. Liu, P. Cooper, P.W. Wypych, Experimental investigation of air entrainment in free-falling particle plumes, *Particul. Sci. Technol.* 25 (2007) 357–373, <https://doi.org/10.1080/02726350701484006>.
- [9] K. Ogata, K. Funatsu, Y. Tomita, Experimental investigation of a free falling powder jet and the air entrainment, *Powder Technol.* 115 (2001) 90–95, [https://doi.org/10.1016/S0032-5910\(00\)00329-6](https://doi.org/10.1016/S0032-5910(00)00329-6).
- [10] Y. Wang, X. Ren, J. Zhao, Z. Chu, Y. Cao, Y. Yang, M. Duan, H. Fan, X. Qu, Experimental study of flow regimes and dust emission in a free falling particle stream, *Powder Technol.* 292 (2016) 14–22, <https://doi.org/10.1016/j.powtec.2016.01.016>.
- [11] Y. Wang, M. Duan, X. Ren, X. Qu, Y. Cao, Y. Yang, H. Fan, Z. Chu, Experimental study of dust emission: comparison between high-temperature and ambient-temperature materials, *Powder Technol.* 301 (2016) 1321–1329, <https://doi.org/10.1016/j.powtec.2016.08.014>.
- [12] R. Darton, The structure and dispersion of jets of solid particles falling from a hopper, *Powder Technol.* 13 (1976) 241–250, [https://doi.org/10.1016/0032-5910\(76\)85009-7](https://doi.org/10.1016/0032-5910(76)85009-7).
- [13] M.E. Möbius, Clustering instability in a freely falling granular jet, *Phys. Rev. E* 74 (2006), 051304, <https://doi.org/10.1103/PhysRevE.74.051304>.
- [14] J.R. Royer, D.J. Evans, L. Oyarte, Q. Guo, E. Kapit, M.E. Möbius, S.R. Waitukaitis, H.M. Jaeger, High-speed tracking of rupture and clustering in freely falling granular streams, *Nature* 459 (2009) 1110–1113, <https://doi.org/10.1038/nature08115>.
- [15] G. Prado, Y. Amarouchene, H. Kellay, Experimental evidence of a rayleigh-plateau instability in free falling granular jets, *Phys. Rev. Lett.* 106 (2011) 198001, <https://doi.org/10.1103/PhysRevLett.106.198001>.
- [16] Y. Amarouchene, J.F. Boudet, H. Kellay, Capillarylike fluctuations at the interface of falling granular jets, *Phys. Rev. Lett.* 100 (2008) 218001, <https://doi.org/10.1103/PhysRevLett.100.218001>.
- [17] G. Prado, Y. Amarouchene, H. Kellay, Incompressible-compressible transition in falling granular jets, *Europhys. Lett.* 102 (2013) 24006, <https://doi.org/10.1209/0295-5075/102/24006>.
- [18] T.J. Goda, F. Ebert, Three-dimensional discrete element simulations in hoppers and silos, *Powder Technol.* 158 (2005) 58–68, <https://doi.org/10.1016/j.powtec.2005.04.019>.
- [19] C. González-Montellano, A. Ramírez, E. Gallego, F. Ayuga, Validation and experimental calibration of 3d discrete element models for the simulation of the discharge flow in silos, *Chem. Eng. Sci.* 66 (2011) 5116–5126, <https://doi.org/10.1016/j.ces.2011.07.009>.
- [20] V. Vidyapati, S. Subramaniam, Granular flow in silo discharge: discrete element method simulations and model assessment, *Ind. Eng. Chem. Res.* 52 (2013) 13171–13182, <https://doi.org/10.1021/ie303598e>.
- [21] Y. Zhou, P.Y. Lagrée, S. Popinet, P. Ruyer, P. Aussillous, Experiments on, and discrete and continuum simulations of, the discharge of granular media from silos with a lateral orifice, *J. Fluid Mech.* 829 (2017) 459–485, <https://doi.org/10.1017/jfm.2017.543>.
- [22] T. Uchiyama, Numerical analysis of particulate jet generated by free falling particles, *Powder Technol.* 145 (2004) 123–130, <https://doi.org/10.1016/j.powtec.2004.06.004>.
- [23] K.W. Chu, Y. Wang, Q.J. Zheng, A.B. Yu, R.H. Pan, Cfd-dem study of air entrainment in falling particle plumes, *Powder Technol.* 361 (2020) 836–848, <https://doi.org/10.1016/j.powtec.2019.11.026>.
- [24] H. Neau, P. Fede, J. Laviéville, O. Simonin, High performance computing (hpc) for the fluidization of particle-laden reactive flows, *The 14th International Conference on Fluidization -From Fundamentals to Products, 2013*.
- [25] H. Neau, J. Laviéville, O. Simonin, NEPTUNE_CFD high parallel computing performances for particle-laden reactive flows, *7th International Conference on Multi-phase Flow, ICMF 2010, Tampa, FL, May 30–June 4, 2010*.
- [26] H. Neau, M. Pigou, P. Fede, R. Ansart, C. Baudry, N. Mérigoux, J. Laviéville, Y. Fournier, N. Renon, O. Simonin, Massively parallel numerical simulation using up to 36,000 CPU cores of an industrial-scale polydispersed reactive pressurized fluidized bed with a mesh of one billion cells, *Powder Technol.* 366 (2020) 906–924, <https://doi.org/10.1016/j.powtec.2020.03.010>.
- [27] C. Lun, S. Savage, D. Jeffrey, N. Chepurmy, Kinetic theories for granular flow: inelastic particles in couette flow and slightly inelastic particles in a general flowfield, *J. Fluid Mech.* 140 (1984) 223–256.
- [28] G. Balzer, A. Boëlle, O. Simonin, Eulerian gas-solid flow modeling of dense fluidized bed, *FLUIDIZATION VII, Proc International Symposium of the Engineering Foundation 1995*, pp. 1125–1134.
- [29] O. Simonin, Combustion and turbulence in two-phase flows, *Lecture Series 1996-02, Von Karman Institute for Fluid Dynamics, 1996*, (pp. –).
- [30] A. Gobin, H. Neau, O. Simonin, J. Llinas, V. Reiling, J. Seilo, Fluid dynamic numerical simulation of a gas phase polymerisation reactor, *Int. J. Numer. Methods Fluids* 43 (2003) 1199–1220, <https://doi.org/10.1002/flid.542>.
- [31] O. Vermorel, B. Bédard, O. Simonin, T. Poinso, Numerical study and modelling of turbulence modulation in particle laden slab flow, *J. Turbul.* 335 (2003) 75–109, <https://doi.org/10.1088/1468-5248/4/1/025>.
- [32] A. Boëlle, G. Balzer, O. Simonin, Second-order prediction of the particle-phase stress tensor of inelastic spheres in simple shear dense suspensions, *Gas-Particle Flows, ASME FED 1995*, pp. 9–18.
- [33] P. Fede, O. Simonin, A. Ingram, 3D numerical simulation of a lab-scale pressurized dense fluidized bed focussing on the effect of the particle-particle restitution coefficient and particle-wall boundary conditions, *Chem. Eng. Sci.* 142 (2016) 215–235, <https://doi.org/10.1016/j.ces.2015.11.016>.
- [34] P.C. Johnson, P. Nott, R. Jackson, Frictional-collisional equations of motion for particulate flows and their application to chutes, *J. Fluid Mech.* 210 (1990) 501–535, <https://doi.org/10.1017/S0022112090001380>.

- [35] A. Srivastava, S. Sundaresan, Analysis of a frictional-kinetic model for gas-particle flow, *Powder Technol.* 129 (2003) 72–85, [https://doi.org/10.1016/s0032-5910\(02\)00132-8](https://doi.org/10.1016/s0032-5910(02)00132-8).
- [36] L. Bennani, H. Neau, C. Baudry, J. Laviéville, P. Fede, O. Simonin, Numerical simulation of unsteady dense granular flows with rotating geometries, *Chem. Eng. Res. Des.* 120 (2017) 333–347, <https://doi.org/10.1016/j.cherd.2017.01.028>.
- [37] S. Benyahia, Validation study of two continuum granular frictional flow theories, *Ind. Eng. Chem. Res.* 47 (2008) 8926–8932, <https://doi.org/10.1021/ie8003557>.
- [38] S. Schneiderbauer, A. Aigner, S. Pirker, A comprehensive frictional-kinetic model for gas-particle flows: analysis of fluidized and moving bed regimes, *Chem. Eng. Sci.* 80 (2012) 279–292, <https://doi.org/10.1016/j.ces.2012.06.041>.
- [39] S. Chialvo, J. Sun, S. Sundaresan, Bridging the rheology of granular flows in three regimes, *Phys. Rev. E* 85 (2012), 021305, <https://doi.org/10.1103/PhysRevE.85.021305>.
- [40] F. Audard, P. Fede, O. Simonin, E. Bêlut, Numerical analysis of dust emission by powder discharge and jet expansion, Proceedings of the ASME-JSME-KSME Joint Fluids Engineering Division Summer Meeting, July 26–31, 2015, Seoul, Korea, 2015, <https://doi.org/10.1115/AJKFluids2015-32120>, p. V001T32A001.
- [41] D. Gidaspow, *Multiphase Flow and Fluidization: Continuum and Kinetic Theory Descriptions*, Academic Press, 1994.
- [42] W. Beverloo, H. Leniger, J. van de Velde, The flow of granular solids through orifices, *Chem. Eng. Sci.* 15 (1961) 260–269, [https://doi.org/10.1016/0009-2509\(61\)85030-6](https://doi.org/10.1016/0009-2509(61)85030-6).
- [43] A. Carleton, The effect of fluid-drag forces on the discharge of free-flowing solids from hoppers, *Powder Technol.* 6 (1972) 91–96, [https://doi.org/10.1016/0032-5910\(72\)80062-7](https://doi.org/10.1016/0032-5910(72)80062-7).
- [44] R. Brown, J.C. Richards, *Principles of Powder Mechanics*, Pergamon Press, 1970.
- [45] P. Jop, Y. Forterre, O. Pouliquen, A constitutive law for dense granular flows, *Nature* 441 (2006) 727–730, <https://doi.org/10.1038/nature04801>.